Article

Sound velocity of hexagonal close-packed iron to the Earth's inner core pressure

Daijo Ikuta [1] ✉, **Eiji Ohtani** [1] ✉, **Hiroshi Fukui** [2,3], **Takeshi Sakai**[4], **Daisuke Ishikawa**[2,3] **& Alfred Q. R. Baron** [2,3] ✉

Here we determine the compressional and shear wave velocities (v_p and v_s) of hexagonal close-packed iron, a candidate for the main constituent of the Earth's inner core, to pressures above 300 gigapascals using a newly designed diamond anvil cell and inelastic X-ray scattering combined with X-ray diffraction. The present results reveal that the v_p and v_s of the Preliminary reference Earth model (PREM) inner core are 4(±2)% and 36(±17)% slower than those of the pure iron, respectively at the centre of the core. The density and sound velocity of the PREM inner core can be explained by addition of 3(±1) wt% silicon and 3(±2) wt% sulphur to iron–5 wt% nickel alloy. Our suggested inner core composition is consistent with the existing outer core model with oxygen, as the growth of the inner core may have created a secular enrichment of the element in the outer core.

Earth's thermal history can be understood from a perspective of timing and nature of inner core crystallisation. The properties of iron under extreme pressure are of great importance to understand the Earth's inner core. Comparison of the density of hexagonal close-packed (hcp) iron under the core conditions and seismic models, e.g., the Preliminary reference Earth model (PREM)[1] indicates that the inner core is less dense than pure iron suggesting it may contain some light elements[2–4]. The most well-known physical property of the core is the sound velocity, specifically the compressional (v_p) and shear (v_s) wave velocities, derived from seismological observations. However, the sound velocity of pure hcp-iron under core conditions remains debated as there are no experimental results at static pressures comparable to the inner core due to the difficulties in measuring sound velocity under such high-pressure conditions. Thus, the discussion about core properties has had to rely on extrapolations from data at lower pressures[5–11]. Different methods have been proposed to extrapolate the relation between sound velocity and density, including a linear relation, known as Birch's law[2], or a power-law relation[7]. Such differences in extrapolation method contribute to the large deviation reported at high pressures when the sound velocity measurements were limited to a low pressure[7,9,11]. In order to solve this problem, it is indispensable to directly determine the sound velocity under the inner core density and pressure without extrapolation.

The Earth's inner core has a density, ρ, of 12.8–13.1 g cm^{-3} at pressures varying from 330 GPa (inner core boundary, ICB) to 365 GPa (centre of the Earth/core, COE)[1]. Here, we measured v_p of hcp-iron to a ρ of 13.87 g cm^{-3} exceeding the inner core density. The corresponding pressure is 310–327 GPa[3,4,12] depending on the pressure scale. This is the highest static pressure so far achieved for inelastic X-ray scattering (IXS) and in situ X-ray diffraction (XRD) methods at BL43LXU[13] of the RIKEN SPring-8 Center, and indeed with any static measurement of a sound velocity. It was made possible by taking advantage of several developments including an improved design of the diamond anvil cell using a "stepped-bevel" anvil (Supplementary Fig. 1) (similar to Fei et al.[4] or Dewaele et al.[14]) combined with highly optimised X-ray optics with a 5 μm beam size, and special Soller screens[15] specifically optimised to improve the signal to noise ratio for this work. These allowed us to extend the accessible pressure range to that of the inner core. We were also aided by the diamond "cupping" that increased the sample thickness and gave more nearly hydrostatic pressure above 300 GPa (see Methods and Supplementary Figs. 2–3). Based on the measurement of v_p of hcp-iron at the core pressures, we evaluated the velocity deficits between hcp-iron and the PREM inner core and consider a

possible candidate light element composition of the inner core to account for both the v_p and v_s of the PREM.

Results

Sound velocity measurement by inelastic X-ray scattering

Figure 1a shows spectra collected at the highest ρ of 13.87 g cm^{-3} corresponding to 310–327 GPa[3,12]. We identified the IXS peaks for the longitudinal acoustic (LA) mode of hcp-iron and the transverse acoustic (TA) and LA modes of diamond together with an elastic peak (not shown). At the highest pressures, the IXS contributions from the diamond TA mode were close to those of the sample LA mode, thus, we used a Soller screen modified to improve the intensity of the sample LA mode relative to the diamond TA mode. While this reduced the signal to the level of 0.01 s^{-1} for the sample peaks, the signal to noise ratio improved, thus, the contributions could be separated by peak fitting. The phonon dispersion curves of all experimental conditions are shown in Fig. 1b and numerical values are given in Table 1. Typical two-

Fig. 1 | Inelastic X-ray scattering (IXS) spectra and dispersion curves of hexagonal close-packed (hcp) iron. a IXS spectra of hcp-iron at 13.87 g cm^{-3} (corresponding to 310 GPa[3]) for different momentum transfers (Q = 7.76, 9.10, 9.97, and 11.25 nm^{-1}) at ambient temperature by an offset of 0.02 cps in the vertical axis for clarity. The data were fit with peaks for longitudinal acoustic (LA) mode of hcp-iron (blue), the transverse acoustic (TA) and LA mode of diamond (orange and green). **b** The dispersion curves of hcp-iron determined at pressures from 154 to 310 GPa based on the equation of state of hcp-iron[3]. The fitted results were given in Table 1. The data for momentum transfer Q and energy transfer E of TA mode of diamond is plotted as grey asterisks. The error bars represent one standard deviation (1σ) uncertainties and are mostly smaller than the circles.

dimensional XRD image and integrated XRD patterns are shown in Supplementary Fig. 4.

Sound velocity of hexagonal close-packed iron

The v_p of hcp-iron determined in this work are plotted with previous IXS results at lower pressures and ambient temperature[5–8,10] in Fig. 2a. It is clear that a linear v_p–ρ relation, Birch's law[2], is valid for hcp-iron up to 13.87 g cm^{-3}, which covers inner core density regions[1] of 12.8–13.1 g cm^{-3}. We find v_p (m s^{-1}) = 1.162(±0.015) ρ (kg m^{-3}) − 3450(±166) (m s^{-1}) by combining the present results and those of previous IXS results[6,8,10]. The v_p of hcp-iron at 12.8–13.1 g cm^{-3} and ambient temperature is 11.4–11.8 km s^{-1}, which is ~3–4% faster than that of PREM inner core. Figure 2b shows the pressure dependence of v_p of hcp-iron using pressures determined by the equation of state (EoS) by Dewaele et al.[3]. The density, ρ, of hcp-iron at the inner core pressure (330–365 GPa) and ambient temperature is estimated to be 14.1–14.4 g cm^{-3}, which is 9–10% larger than that of the PREM inner core of 12.8–13.1 g cm^{-3}. As determined from our work, v_p of hcp-iron at inner core pressure (330–365 GPa) and ambient temperature is 12.7–13.3 km s^{-1}, which is significantly faster (~15–18%) than that of the PREM inner core. The present sound velocity measurements of hcp-iron to the core density of 13.87 g cm^{-3} showed a linear v_p–ρ relation is good for the extrapolation of v_p of hcp-iron[6–8] to the PREM inner core density. In fact, given the extended data range now available, extrapolations both by a linear and exponential relations provide similar values of the sound velocity for the inner core density, eliminating the previous contradictions originating from different extrapolation methods. This shows the importance of performing measurements to the inner core density.

We parameterise the temperature dependence[16] of the Birch's law as:
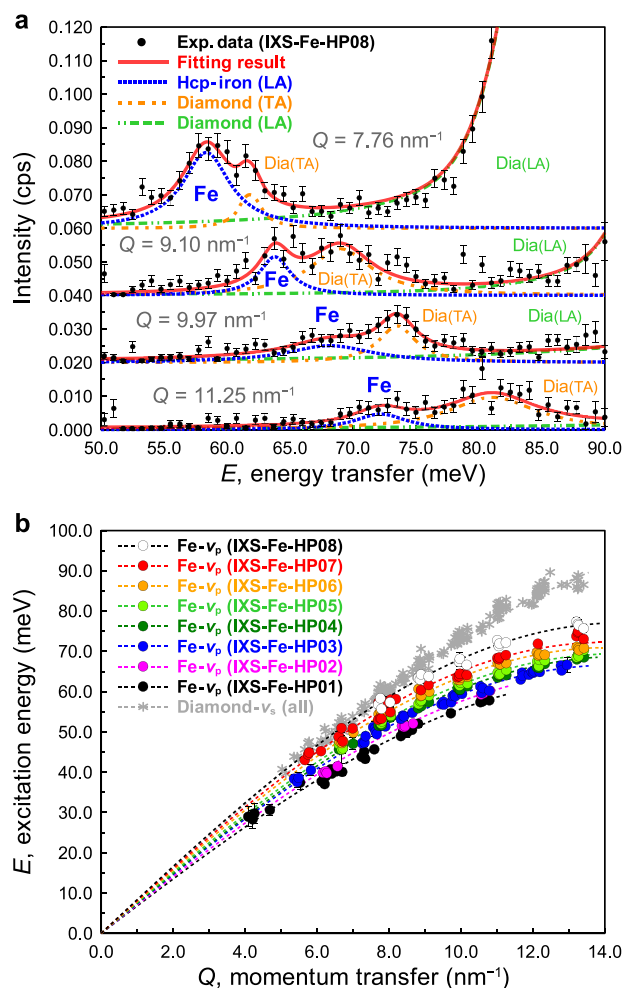
$$v_p = A\rho - B - C(T - T_0)(\rho_x - \rho), \qquad (1)$$

where A, B, C, and ρ_x are the parameters of the relation, T is temperature, and T_0 is ambient temperature, i.e., 300 K. The effect of temperature on the v_p–ρ relation, i.e., the Birch's law, of hcp-iron at high temperature is re-evaluated by combining the present results with previous measurements at high temperature[6,8,16]. This is shown in Fig. 3a. We find the updated parameters, A = 1.162(±0.015) m^4 kg^{-1} s^{-1}, B = 3450(±166) m s^{-1}, C = 2.5(±0.2) × 10^{-5} m^4 kg^{-1} s^{-1} K^{-1}, and ρ_X = 19.2(±0.3) × 10^3 kg m^{-3}. Our results for the v_p–ρ relation at high temperature are consistent with the ab initio calculations made by Vocadlo et al.[17] and Martorell et al.[18]: their theoretical results provide slightly higher v_p at the inner core conditions, but still within the uncertainty of our estimation.

The v_s–ρ relation of hcp-iron is shown in Fig. 3b, where v_s is related to v_p and the adiabatic bulk modulus (K_S) as follows:

$$K_S = \rho\left(v_p^2 - \frac{4}{3}v_s^2\right). \qquad (2)$$

The details of estimation of v_s are given in Methods. There are discrepancies in v_p–ρ and v_s–ρ relations of hcp-iron among ab initio calculations[17–19] as discussed by Bouchert et al.[19]. Our result is generally consistent with calculations by Vocadlo et al.[17] and Martorell et al.[18].

Figure 4 shows the v_p–ρ and v_s–ρ relations for hcp-iron at ICB and COE at 300 K and 6000 K based on the EoS of Dewaele et al.[3] compared to the values of the PREM inner core[1]. Pure hcp-iron has 2(±2)% higher v_p and 29(±17)% higher v_s at the ICB, and 4(±2)% higher v_p and 36(±17)% higher v_s at the COE, respectively, compared to those of the PREM inner core with a typical estimated inner core temperature of 6000 K (e.g., refs. [20–22]). The present v_p deficit is smaller than that estimated previously by Sakamaki et al.[16]. A large v_s deficit compared to the v_p deficit of the PREM inner core relative to hcp-iron is an important constraint on the sound velocity deficits determined by direct

Table 1 | Experimental conditions and results

Run-no.	ρ, density (g cm^{-3})	v_p, compress. wave velocity (km s^{-1})	$Q_{max}(v_\mathrm{p})$ (nm^{-1})	$P_{(Dewaele, 2006)}$ (GPa)[3]	$P_{(Fei, 2016)}$ (GPa)[4]	$P_{(Smith, 2018)}$ (GPa)[12]
IXS-Fe-HP01	11.95 (±0.07)	10.32 (±0.10)	14.7 (±0.5)	154	155	157
IXS-Fe-HP02	12.27 (±0.06)	10.72 (±0.19)	14.5 (±0.5)	177	177	181
IXS-Fe-HP03	12.63 (±0.05)	11.13 (±0.12)	14.3 (±0.4)	203	204	210
IXS-Fe-HP04	12.80 (±0.06)	11.30 (±0.14)	14.5 (±0.2)	217	218	224
IXS-Fe-HP05	12.97 (±0.05)	11.58 (±0.11)	14.3 (±0.2)	231	232	239
IXS-Fe-HP06	13.21 (±0.08)	11.99 (±0.10)	14.1 (±0.2)	250	252	261
IXS-Fe-HP07	13.52 (±0.07)	12.30 (±0.10)	14.1 (±0.2)	278	280	291
IXS-Fe-HP08	13.87 (±0.07)	12.69 (±0.16)	14.1 (±0.2)	310	314	327

static measurements at core densities. This provides a strong constraint for estimation of the light element contents in the inner core.

Discussion

The inner core v_p and v_s deficits reported in this work together with the density deficit[3] of the PREM inner core compared to pure hcp-iron provides important constraints on the composition of the inner core. As pure iron cannot explain the density and velocity of the PREM, many studies on physical properties of iron alloys or iron compounds were performed to account for those deficits and concluded that light elements play a major role to account for the deficits[2–4].

Geochemical studies[23] have suggested silicon and sulphur may be the major light elements in the core. A numerical study[24] clarified the partitioning behaviour of silicon, sulphur, and oxygen between solid and liquid iron, and revealed a strong partitioning of oxygen into the liquid outer core, indicating the silicon and sulphur bearing inner core with oxygen depletion. The high sound velocity of FeO suggests oxygen is not a major light element of the inner core (Supplementary Fig. 5). Therefore, a reasonable combination of light elements to account for the PREM inner core may be the mixture of the three-endmember components of iron (or iron–nickel alloy), iron–silicon alloy (e.g., Fe$_{0.89}$Si$_{0.11}$), and iron–sulphur compound (e.g., Fe$_3$S).

Figure 5 summaries the v_p–ρ (Fig. 5a) and v_s–ρ (Fig. 5b) relations of hcp-iron, iron alloys (Fe$_{0.89}$Si$_{0.11}$ and Fe$_{0.86}$Ni$_{0.14}$), and iron–light element compounds (Fe$_3$S) under the inner core conditions (330–365 GPa, 6000 K). We derive the properties v_p, v_s, and ρ at ICB and COE using previous sound velocity measurements and EoSs[25–30] (details are given in Methods). The temperature dependence of v_p for Fe$_{0.89}$Si$_{0.11}$ was reported by Sakairi et al.[25], and those of Fe$_{0.86}$Ni$_{0.14}$ and Fe$_3$S are assumed to be the same as that of hcp-iron in this work.

The triangles of these endmember components at both ICB and COE in Fig. 5 (lighter and darker magenta colours indicate ICB and COE conditions, respectively) can account for ρ, v_p, and v_s of the PREM inner core. The uncertainties associated with velocity measurements and the EoS of hcp-iron are shown in the figure. When we consider iron–silicon–sulphur alloy, ρ, v_p, and v_s of the PREM inner core can be accounted for by addition of 4(±1) wt% silicon and 3(±1) wt% sulphur at ICB and 4(±1) wt% silicon and 4(±1) wt% sulphur at COE, assuming Fe$_{0.89}$Si$_{0.11}$ and Fe$_3$S endmembers have the same uncertainties as hcp-iron. Assuming that the inner core is iron with a homogeneous distribution of light elements, the best estimation of the light elements in the whole inner core is 4(±1) wt% silicon and 3(±2) wt% sulphur. However, meteorite composition and geochemistry strongly suggest that the core contains a substantial amount of nickel[23]. When we consider the nickel content of the inner core has the chondritic Ni/Fe ratio (e.g., ref. 31) as 0.06, ρ, v_p, and v_s of the PREM inner core can be accounted for by addition of 3(±1) wt% silicon and 3(±1) wt% sulphur at ICB and 2(±1) wt% silicon and 4(±1) wt% sulphur at COE to the metallic iron–nickel–silicon–sulphur alloy (~5 wt% nickel, which is the chondritic Ni/Fe ratio). There may be some heterogeneities in the light element content between ICB and COE, but those are within our

uncertainties. Assuming that the inner core has a homogeneous distribution of light elements with the chondritic Ni/Fe ratio, the best estimation of the light elements in the whole inner core then becomes 3(±1) wt% silicon and 3(±2) wt% sulphur.

Our estimations of the silicon and sulphur contents of the inner core are based on the deficits of compressional and shear velocities and density, whereas most previous estimations were based only on the density deficit of the inner core, and occasionally, the v_p deficit[10,32,33]. Therefore, our results are more definite compared to the previous estimations. Additionally, previous studies provided contradictory estimates in silicon and sulphur contents in the inner core, ~5–8 wt%[34,35] and ~1–4 wt%[10,32,33] in silicon content, whereas the sulphur content varies from 1.3 to 3.7 wt%[36,37]. The present analysis suggests that both silicon and sulphur may be needed to account for the properties of the inner core. McDonough[23] estimated the amount of silicon and sulphur of the bulk core to be 6 wt% and 1.9 wt%, respectively, from geochemical constraints. The numerical study by Alfe et al.[24] suggested existence of very small amount oxygen around 0.3 wt % (0.2 mol%), and silicon and/or sulphur around 4.5–5 wt% (8.5 mol%) in the inner core to account for the density of the PREM inner core. The present mineral physics estimate of silicon and sulphur contents in the inner core, 3(±1) wt% silicon and 3(±2) wt% sulphur with ~5 wt% nickel, is consistent with the geochemical and numerical estimations[23,24,38].

Martorell et al.[18] introduced the pre-melting effect in hcp-iron to account for the v_p and v_s of the PREM inner core. However, our analysis indicates such an anomalous effect is not required and introduction of both silicon and sulphur components can explain the inner core deficit of v_p, and v_s. Although the solid–liquid partitioning data of iron alloy is not available under the inner core conditions, previous data suggested very small value of partition coefficient (D) of oxygen [D(O) ~0, e.g., refs. 24,39] and sulphur [D(S) = 0.4–0.8, e.g., refs. 39,40], and very weak partitioning of silicon between solid and liquid iron alloys [D(Si) ~1, e.g., refs. 41–43]. Therefore, present silicon and sulphur abundances in the inner core is consistent with the outer core containing a large amount of oxygen with a limited amount of sulphur and silicon by ab initio calculations[21,24,44]. The difference in the light element contents such as oxygen, sulphur, and silicon between inner and outer cores suggests enrichment of oxygen in the outer core during crystallisation of the inner core.

The v_p–ρ and v_s–ρ relations of hcp-iron, iron alloys (Fe$_{0.89}$Si$_{0.11}$, 6 wt% silicon alloy and Fe$_{0.86}$Ni$_{0.14}$, 15 wt% nickel alloy), and iron–light element compounds (Fe$_7$C$_3$, Fe$_3$C, Fe$_3$S, FeH, and FeO) under the inner core conditions (330–365 GPa, 6000 K) are summarised in Supplementary Fig. 5. We derive the properties v_p, v_s, and ρ at ICB and COE using previous sound velocity measurements and EoSs[25–30,45–50] (details are given in Methods) and assuming a similar temperature dependence of v_p as that of hcp-iron determined above, except for Fe$_{0.89}$Si$_{0.11}$, Fe$_7$C$_3$, Fe$_3$C, and FeO, which were determined experimentally[25,45,46,50]. It is not possible to rule out other compositions such as carbon[45,46,51] and hydrogen[52–54] since in most cases the uncertainties of estimations of v_p and v_s in the iron–light element compounds are greater than those of
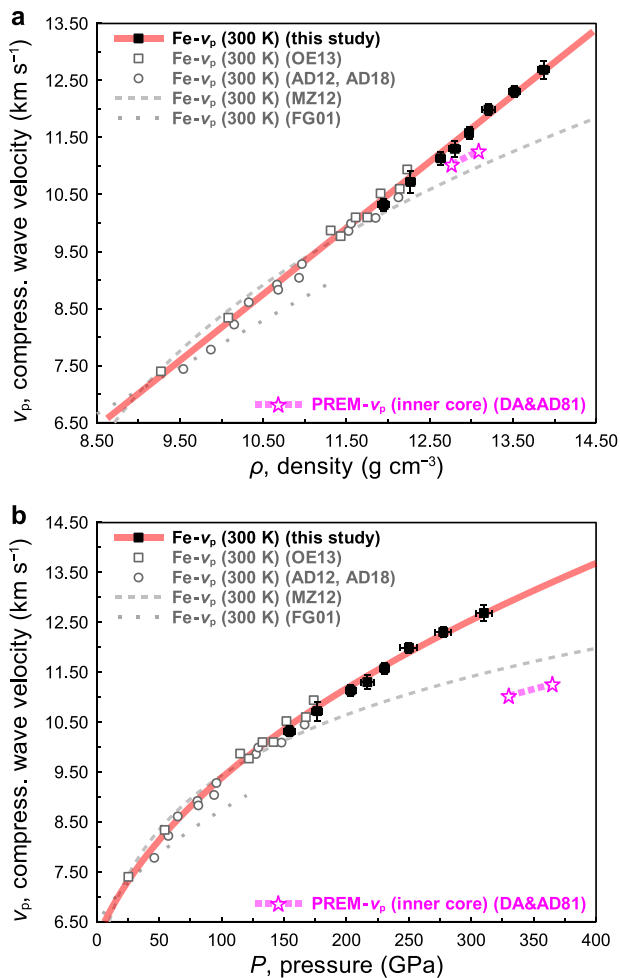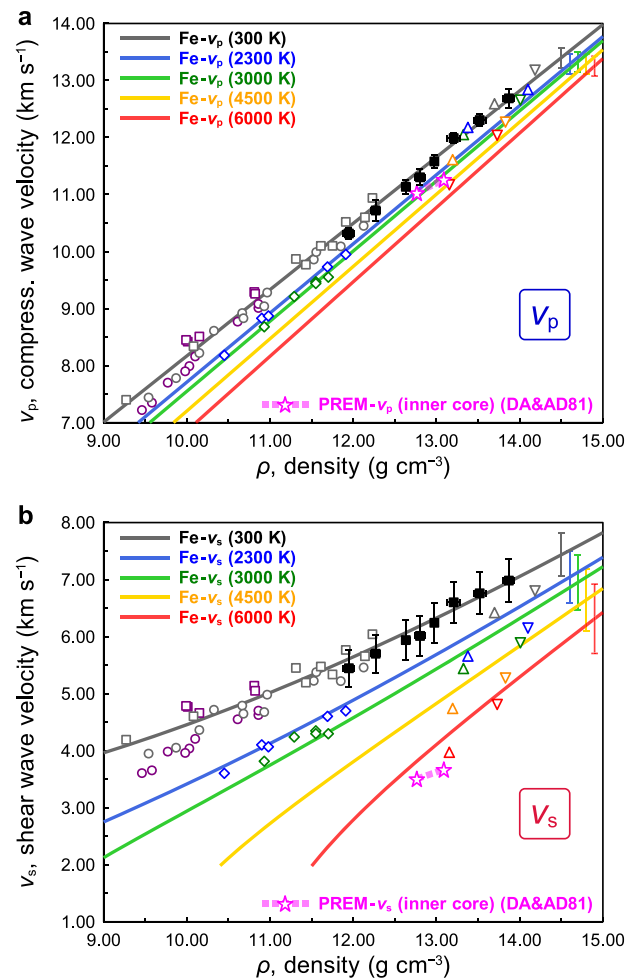
Fig. 2 | Compressional wave velocity (v_p) of hexagonal close-packed (hcp) iron at high pressure. a The v_p–ρ relation of hcp-iron at ambient temperature. Solid squares are the results of this work; open squares from Ohtani et al. (OE13)[8]; circles from Antonangeli et al. (AD12, AD18)[6,10]; a dashed curve extrapolated by a power-law relation from Mao et al. (MZ12)[7]; and a dotted curve from Fiquet et al. (FG01)[5,11]. The magenta dashed curve with stars is the Preliminary reference Earth model (PREM) inner core (DA&AD81)[1]. **b** The pressure dependency of v_p of hcp-iron at ambient temperature. The pressures were evaluated by the equation of state of hcp-iron by Dewaele et al.[3] The symbols are the same as those in Fig. 2a. The error bars represent 1σ uncertainties.

Fig. 3 | Compressional (v_p) and shear (v_s) wave velocities of hexagonal close-packed (iron) at high pressure and temperature. a The v_p–ρ relation, i.e., Birch's law[2], for hcp-iron at different temperature. We include the ambient temperature data of this work (black solid squares) and Ohtani et al. (grey open squares)[8], Antonangeli et al. (grey circles)[6,10], and high temperature data by Sakamaki et al. (blue diamonds: 2300 K, green diamonds: 3000 K)[16], Ohtani et al. (purple squares: 400–1000 K)[8] and Antonangeli et al. (purple circles: 700–1110 K)[6] for deriving the temperature dependence. The theoretical data (coloured open triangles, grey: 0 K, blue: 2300 K, green 3000 K, orange: 4500 K, and red: 5500 K)[17,18] and the Preliminary reference Earth model (PREM) inner core (a magenta curve with stars, DA&AD81)[1] are shown for comparison. Coloured lines represent the v_p–ρ relations derived from the experimental data of this work with other inelastic X-ray scattering (IXS) experimental data[6,8,16] (grey: 300 K, blue: 2300 K, green 3000 K, orange: 4500 K, and red: 6000 K). **b** The v_s–ρ relation at different temperatures. The calculation of the v_s for the IXS experiments are given in the Methods. The curves showing the v_s–ρ relations are derived from the linear v_p–ρ relations in Fig. 3a and the equation of state[3]. Symbols given in this figure are the same as those of Fig. 3a. The error bars represent 1σ uncertainties.

the present results on pure hcp-iron due to large extrapolations. Recently, Wang et al.[53] and He et al.[54] suggested existence of the superionic iron–light element compounds, including hydrogen to account for the large reduction of v_s of the inner core compared to hcp-iron. If we consider the existence of such superionic iron–light element compounds, the alloying light elements in the inner core might contain hydrogen with smaller amounts of other light elements than those estimated here.

Methods
Starting material and high-pressure generation
The rhenium gasket material was a 250 μm thick foil, 99.97% purity, from Alfa Aesar, that was pre-compressed to a thickness of ~10 μm. A hole of 15 μm diameter was drilled for the sample chamber. Iron powder (99.99% purity from Wako Chemicals) was placed in the rhenium gasket hole without pressure medium. Double bevel diamond anvils with a culet size of 50 μm were used with a rhenium gasket to generate the pressure up to 250–278 GPa[3,4,12]. Higher pressures were generated by the improved "stepped bevel" diamond anvil. The

stepped bevel anvils with a culet size of 30 μm was made by machining a flat surface of 70 μm in diameter with a depth of ~3 μm outside the 30 μm culet of (100)-oriented single crystalline double bevel anvils, using a dual focused ion beam (FIB)–scanning electron microscope (SEM) module (Scios). Supplementary Fig. 1a shows the shape of the anvil determined by the field emission SEM after the machining. Supplementary Fig. 1b shows the microscopic image under maximum pressure (310 GPa[3], 315 GPa[4], and 327 GPa[12]). The anvil obviously keeps the stepped bevel shape with the sample chamber of ~20 μm (expanded from the starting size of 15 μm), which is brightest area.
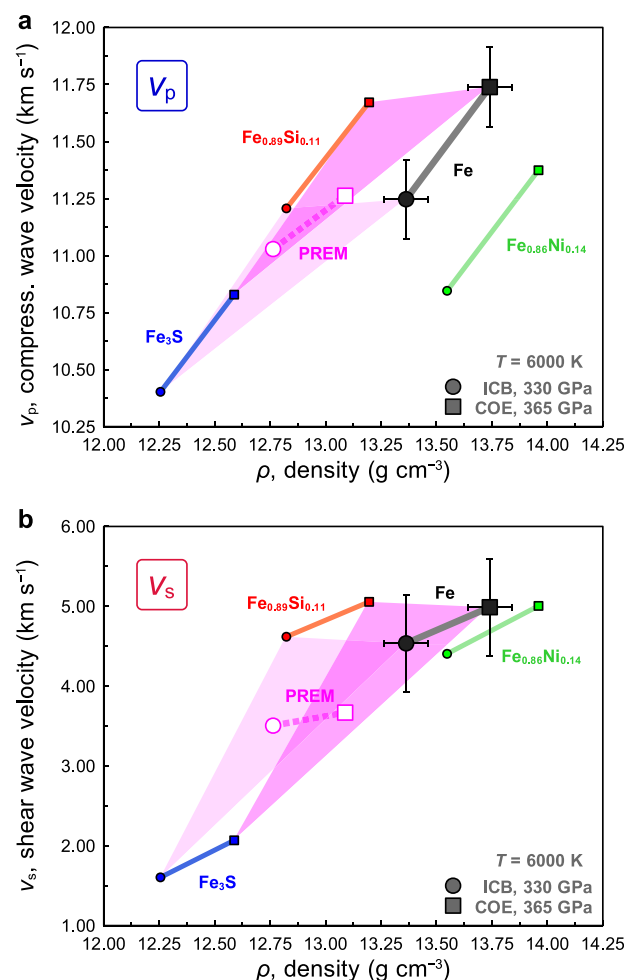
Supplementary Fig. 2a shows iron sample or rhenium gasket thickness distribution of stepped bevel anvil compared with a double
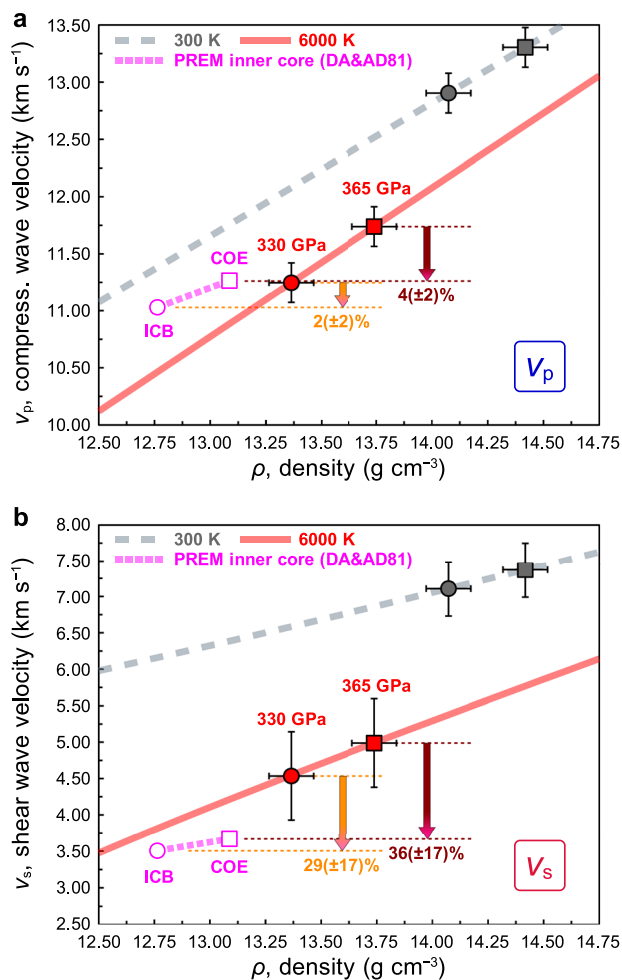
Fig. 4 | Comparison of density–velocity relations of hexagonal close-packed (hcp) iron at inner core conditions with Preliminary reference Earth model (PREM). The v_p deficit (**a**) and the v_s deficit (**b**) in the inner core. The v_p and v_s of the PREM inner core (DA&AD81)[1] compared to those of hcp-iron at ambient temperature (grey dashed curves) and 6000 K (red curves: fitted v_p–ρ and v_s–ρ relations) at 330 GPa (inner core boundary, ICB, and circle symbols) and 365 GPa (centre of the Earth/core, COE, and square symbols). The equation of state of hcp-iron by Dewaele et al.[3] was used for the calculation. The v_p deficit and the v_s deficit are 2(±2)% and 29(±17)% at the ICB, and 4(±2)% and 36(±17)% at the COE, respectively. The error bars represent 1σ uncertainties.

Fig. 5 | Comparison of v–ρ relations of hexagonal close-packed (hcp) iron, iron alloys $Fe_{0.89}Si_{0.11}$ and $Fe_{0.86}Ni_{0.14}$, and iron sulphur compound Fe_3S with Preliminary reference Earth model (PREM) at the inner core boundary (ICB, 330 GPa, and 6000 K) and centre of the Earth/core (COE, 365 GPa, and 6000 K) conditions. The v_p–ρ (**a**) and the v_s–ρ (**b**) relations of each material. The circle and square symbols indicate ICB and COE conditions, respectively. The coloured symbols are as follows: black is hcp-iron from this study (pressure is evaluated by the Dewaele et al.[3]), red is $Fe_{0.89}Si_{0.11}$ (6 wt% silicon)[25,26], green is $Fe_{0.86}Ni_{0.14}$ (15 wt% nickel)[27,28], blue is Fe_3S[29,30], and magenta (open symbol) is PREM[1]. The v–ρ relations for hcp-iron at the ICB and COE conditions are determined by this work (see text and Methods). The v–ρ relations of other iron alloys and iron compound are calculated from previous studies on sound velocity and equations of state[25–30], and the present temperature dependence of hcp-iron (details are in Methods) for $FeNi_{0.15}$ and Fe_3S. The magenta triangles represent the potential v–ρ relations of the iron compounds consisting of three endmembers (hcp-iron, $Fe_{0.89}Si_{0.11}$, and Fe_3S) (lighter and darker colours indicate ICB and COE conditions, respectively). The error bars represent 1σ uncertainties for hcp-iron.

bevel anvil at 278 GPa[3] derived from X-ray absorption. For stepped bevel anvil, the shape of the sample is slightly more "cupped" compared to the double bevel anvil. Supplementary Fig. 2b shows the integrated XRD profiles at 278 GPa[3] in sample position and 5, 10, 20, and 35 μm off-centred positions. Pressure decreases by ~10 GPa and ~20 GPa at 5 μm and 10 μm off-centred positions, respectively, a pressure distribution similar to the diamond anvil used in refs. 4,14. In ideal hcp-iron, 101 peak has maximum intensity, and 100 and 002 peaks have almost same intensities. However, in the XRD profile by a double bevel anvil, there is no obvious 002 peak, and 100 peak is stronger than 101 peak. This indicates the pressure generation by a double bevel anvil causes strong preferred orientation. Compared with the pressure generation by a double bevel anvil, XRD profiles by a stepped bevel anvil indicates more quasi-hydrostatic conditions, because there is 002 peak and 101 peak has maximum intensity. In high-pressure diamond anvil cell (DAC) experiments, the effect of uniaxial compression on preferred orientation should be considered[16,55–57]. Typical profiles of crystal axis concentrations are shown in Supplementary Fig. 3a by stereographic projection. Supplementary Fig. 3b shows the experimentally measured distributions of

crystal direction (due to preferred orientation) at 278 GPa of both stepped bevel and double bevel anvils, with calculated v_p anisotropy from the theoretical data[17,18]. The experimental preferred orientation by a stepped bevel anvil shows weak preferred orientation and the angle between the c-axis and the momentum transfer is widely distributed, from 30 to 90 degrees. On the other hand, the experimental preferred orientation by a double bevel anvil shows strong preferred orientation and c-axis of hcp-structure is almost parallel with the compressional direction (and also incident X-ray beam). The effect of these experimental preferred orientations and calculated v_p anisotropy[17,18] on the sound velocity measurement is shown in Supplementary Fig. 3c. The effects of anisotropy on v_p in stepped bevel anvil experiments and double bevel anvil experiments are <0.5% and

<1.3%, respectively. The effect of anisotropy on v_p is within the uncertainty of the present v_p measurement shown in Table 1. The anisotropy is smaller in stepped bevel anvil experiments, although it is still small in double bevel anvil experiments. Therefore, our experimental v_p can be estimated to be almost consistent with the v_p with a random orientation.

IXS–XRD measurement

The v_p and density, ρ, of hcp-iron were measured using a DAC combined with IXS and XRD methods at BL43LXU[13] of SPring-8. The Si (9 9 9) reflection at 17.79 keV provided a resolution of 2.8 meV. A fine focused beam of 5 µm × 5 µm by a multilayer Kirkpatrick-Baez mirror pair[15] was employed for the IXS–XRD measurements. The energy of the LA mode of hcp-iron, and the LA and TA modes of diamond from DAC were extracted by fitting with combination of Gaussian and Lorentzian functions, so called pseudo-Voigt function. It was difficult to separate the signal of the LA mode of the sample from the TA mode of diamond because the IXS signal from diamond was large compared to the sample in the DAC at pressures above 100 GPa. Thus, in order to reduce the background from diamond and to improve signal to noise ratio, we installed a Soller screen[15] downstream of the DAC. For the higher density measurements presented here (>13.5 g cm^{-3}), the Soller screen was modified from that described in ref. 15 in order to improve the signal-to-noise ratio. While this modification (reduction in the slit width) also reduced the signal, and therefore led to longer counting times, the trade-off was deemed acceptable to carry out the experiments. We note that results with different diamond anvil cell types and with different Soller screens were consistent. In particular, the IXS experiments at 278 GPa[3] were performed in multiple configurations and the observed peak positions were consistent within the error as shown in Fig. 1b. The in situ XRD patterns of hcp-iron were collected under the same optical setup at BL43LXU beamline before and after the IXS measurements using a flat panel (FP) detector (C9732DK, Hamamatsu Photonics). The distance between the sample and the flat panel detector was calibrated with a cerium dioxide standard (NIST, National Institute of Standards and Technology). The XRD patterns were analysed using the software packages by Seto et al.[58,59] and the lattice parameters, densities, and the information of preferred orientation for hcp-iron were determined from the XRD patterns (Supplementary Figs. 2–4). The experimental pressure was evaluated by the EoS of hcp-iron[3,4,12] (Table 1).

The relation between the excitation energy, v_p and the momentum transfer is given by

$$E = \frac{h v_p Q_{max}}{\pi^2} \sin\left(\frac{\pi Q}{2 Q_{max}}\right), \tag{3}$$

where E is excitation energy, h is Plank's constant, Q is momentum transfer, and Q_{max} is the averaged distance to the edge of the first Brillouin zone, including the effect of the preferred orientation[55,60]. To obtain the v_p from the IXS spectra, the dispersion was fit with the above sine equation[5–10,16,25,29,33,46,47,50,55,57]. A weighted least-squares method was used with v_p and Q_{max} as free parameters.

Estimation of sound velocities (v_p and v_s) at high pressure and temperature

The v_p of iron, iron alloys, and iron–light element compounds at high pressure is interpolated/extrapolated by a linear relation (Birch's law[2]) as

$$v_p = A\rho - B \tag{4}$$

from present and previous wave velocity measurements: hcp-iron (this study), Fe$_{0.89}$Si$_{0.11}$ (6 wt% silicon)[25], Fe$_{0.86}$Ni$_{0.14}$ (15 wt% nickel)[27],

Fe$_3$S[29], Fe$_7$C$_3$[45], Fe$_3$C[46], FeH[47], and FeO[50]. The v_p of iron at high temperature is parameterised by using high temperature data[6,8,16] combining the present new Birch's law of hcp-iron at ambient temperature with the following form[16]:

$$v_p = A\rho - B - C(T - T_0)(\rho_x - \rho), \tag{5}$$

where A, B, C, and ρ_x are the parameters of the relation, T is temperature, and T_0 is ambient temperature, i.e., 300 K. We use the temperature dependency measured experimentally for Fe$_{0.89}$Si$_{0.11}$[22], Fe$_7$C$_3$[45], Fe$_3$C[46], and FeO[50]. The temperature dependency of pure iron is used in Fe$_{0.86}$Ni$_{0.14}$[27], Fe$_3$S[29], and FeH[47] as their direct temperature dependencies were not available. Thus, it should be noted that estimations of temperature dependency of those compounds are less reliable.

The v_s of iron, iron alloys, and iron–light element compounds are derived by using present and previous wave velocity measurements and EoSs: hcp-iron[3,12], Fe$_{0.89}$Si$_{0.11}$[25,26], Fe$_{0.86}$Ni$_{0.14}$[27,28], Fe$_3$S[29,30], Fe$_7$C$_3$[45], Fe$_3$C[46], FeH[47–49], and FeO[50]. v_s is related to v_p and the adiabatic bulk modulus (K_S) as follows:

$$K_S = \rho\left(v_p^2 - \frac{4}{3}v_s^2\right). \tag{6}$$

Also, K_S and the isothermal bulk modulus (K_T) are defined as follows:

$$K_T = K_S - \rho\gamma^2 c_V T, \tag{7}$$

where ρ is the density, γ is the Grüneisen parameter, and c_V is the molar heat capacity at constant volume. c_V is derived from the derivative of the molar internal energy (or the pressure) with respect to the temperature,

$$c_V = \left(\frac{\partial U}{\partial T}\right)_V = \frac{V}{\gamma}\left(\frac{\partial P}{\partial T}\right)_V, \tag{8}$$

where U is the molar internal energy, and V is the molar volume[60]. The P–V–T relations and the thermodynamic Grüneisen parameter γ were given by the EoSs of the alloys and compounds[3,4,26,28,30,45,46,48,50] with Mie–Grüneisen–Debye model. c_V and K_T–K_S conversion are derived from above thermodynamic relations with each EoS parameters.

Differences due to pressure evaluations by different equations of state

Pressure value depends on the EoS (e.g., present maximum experimental density of 13.87 g cm^{-3} correspond to 310 GPa[3], 314 GPa[4], and 327 GPa[12]), thus, we need to consider the differences due to EoS. To consider the effects of pressure scales, we compare ρ, v_p, and v_s deficits and amounts of light elements by using another iron EoS of Smith et al. (Smith-EoS)[12] to the present results based on the EoS of Dewaele et al. (Dewaele-EoS)[3], because pressures by Smith-EoS have larger discrepancies than those evaluated by the EoS of Fei et al.[4]. Supplementary Fig. 6 shows the pressure dependence of v_p of hcp-iron at ambient temperature, in which pressures are evaluated by the Smith-EoS. Compared to the result by Dewaele-EoS, the maximum experimental pressure was evaluated as 327 GPa, which is 17 GPa higher than that by Dewaele-EoS. As mentioned above, v_s is derived from v_p and EoS, Supplementary Fig. 7 shows the v_s–ρ relation of hcp-iron derived by using Smith-EoS. The results with Smith-EoS shows better consistency with theoretical results[6,10] than that of Dewaele-EoS, however, both do not show significant deviations and are within the uncertainty. Supplementary Fig. 8 shows the v_p–ρ and v_s–ρ relations for pure hcp-iron at ICB and COE depending on the Smith-EoS and those of the PREM inner core. The v_p and v_s deficits by Smith-EoS are 1(±1)% and 24(±16)% at ICB

and 4(±2)% and 29(±15)% at COE, respectively. Therefore, we conclude that there are no significant deviations in the discussions of v_p and v_s deficits.

Data availability
All data used in this study are presented in the text, Methods, and supplementary information. Experimental conditions and results are summarised in Table 1. The data used to produce figures can be accessed from the public repository Zenodo.

Code availability
We used IPAnalyzer/PDindexer/ReciPro software package[58,59], which is available at https://github.com/seto77/.

References
1. Dziewonski, A. M. & Anderson, D. L. Preliminary reference Earth model. *Phys. Earth Planet. Inter.* **25**, 297–356 (1981).
2. Birch, F. Density and composition of mantle and core. *J. Geophys. Res.* **69**, 4377–4388 (1964).
3. Dewaele, A. et al. Quasihydrostatic equation of state of iron above 2 Mbar. *Phys. Rev. Lett.* **97**, 215504 (2006).
4. Fei, Y., Murphy, C., Shibazaki, Y., Shahar, A. & Huang, H. Thermal equation of state of hcp-iron: Constraint on the density deficit of Earth's solid inner core. *Geophys. Res. Lett.* **43**, 6837–6843 (2016).
5. Fiquet, G., Badro, J., Guyot, F., Requardt, H. & Krisch, M. Sound velocities in iron to 110 gigapascals. *Science* **291**, 468–471 (2001).
6. Antonangeli, D. et al. Simultaneous sound velocity and density measurements of hcp iron up to 93 GPa and 1100 K: An experimental test of the Birch's law at high temperature. *Earth Planet. Sci. Lett.* **331–332**, 210–214 (2012).
7. Mao, Z. et al. Sound velocities of Fe and Fe-Si alloy in the Earth's core. *Proc. Natl Acad. Sci. USA* **109**, 10239–10244 (2012).
8. Ohtani, E. et al. Sound velocity of hexagonal close-packed iron up to core pressures. *Geophys. Res. Lett.* **40**, 5089–5094 (2013).
9. Liu, J. et al. Seismic parameters of hcp-Fe alloyed with Ni and Si in the Earth's inner core. *J. Geophys. Res.* **121**, 610–623 (2016).
10. Antonangeli, D. et al. Sound velocities and density measurements of solid hcp-Fe and hcp-Fe-Si (9 wt.%) alloy at high pressure: Constraints on the Si abundance in the Earth's inner core. *Earth Planet. Sci. Lett.* **482**, 446–453 (2018).
11. Antonangeli, D. & Ohtani, E. Sound velocity of hcp-Fe at high pressure: Experimental constraints, extrapolations and comparison with seismic models. *Prog. Earth Planet. Sci.* **2**, 3 (2015).
12. Smith, R. F. et al. Equation of state of iron under core conditions of large rocky exoplanets. *Nat. Astron.* **2**, 452–458 (2018).
13. Baron, A. Q. R. in *Synchrotron Light Sources and Free-Electron Lasers* (eds. Jaeschke, E., Khan, S., Schneider, J. R. & Hastings, J. B.) 1643–1757 (Springer International Publishing, 2016).
14. Dewaele, A., Loubeyre, P., Occelli, F., Marie, O. & Mezouar, M. Toroidal diamond anvil cell for detailed measurements under extreme static pressures. *Nat. Commun.* **9**, 2913 (2018).
15. Baron, A. Q. R., Ishikawa, D., Fukui, H. & Nakajima, Y. Auxiliary optics for meV-resolved inelastic x-ray scattering at SPring-8: Microfocus, analyzer masks, Soller slit, soller screen, and beam position monitor. *AIP Conf. Proc.* **2054**, 020002 (2019).
16. Sakamaki, T. et al. Constraints on Earth's inner core composition inferred from measurements of the sound velocity of hcp-iron in extreme conditions. *Sci. Adv.* **2**, e1500802 (2016).
17. Vocadlo, L., Dobson, D. P. & Wood, I. G. Ab initio calculations of the elasticity of hcp-Fe as a function of temperature at inner-core pressure. *Earth. Planet. Sci. Lett.* **288**, 534–538 (2009).
18. Martorell, B., Vocadlo, L., Brodholt, J. & Wood, I. G. Strong pre-melting effect in the elastic properties of hcp-Fe under inner-core conditions. *Science* **342**, 466–468 (2013).
19. Bouchet, J., Bottin, F., Antonangeli, D. & Morard, G. Sound velocities and thermodynamical properties of hcp iron at high pressure and temperature. *J. Phys. Condens. Matter* **34**, 344002 (2022).
20. Stixrude, L., Wasserman, E. & Cohen, R. E. Composition and temperature of Earth's inner core. *J. Geophys. Res.* **102**, 24729–24739 (1997).
21. Alfe, D., Gillan, M. J. & Price, G. D. Temperature and composition of the Earth's core. *Contemp. Phys.* **48**, 63–80 (2007).
22. Anzellini, S., Dewaele, A., Mezouar, M., Loubeyre, P. & Morard, G. Melting of iron at Earth's inner core boundary based on fast x-ray diffraction. *Science* **340**, 464–466 (2013).
23. McDonough, W. F. in *Treatise on Geochemistry 2nd Edition Vol. 3: The Mantle and Core* (eds. Holland, H. D. & Turekian, K. K.) 559–577 (Elsevier, 2014).
24. Alfe, D., Gillan, M. J. & Price, G. D. Composition and temperature of the Earth's core constrained by combining ab initio calculations and seismic data. *Earth Planet. Sci. Lett.* **195**, 91–98 (2002).
25. Sakairi, T. et al. Sound velocity measurements of hcp Fe-Si alloy at high pressure and high temperature by inelastic x-ray scattering. *Am. Mineral.* **103**, 85–90 (2018).
26. Edmund, E. et al. Velocity-density systematics of Fe-5wt%Si: Constraints on Si content in the Earth's inner core. *J. Geophys. Res.* **124**, 3436–3447 (2019).
27. Wakamatsu, T., Ohta, K., Yagi, T., Hirose, K. & Ohishi, Y. Measurements of sound velocity in iron-nickel alloys by femtosecond laser pulses in a diamond anvil cell. *Phys. Chem. Miner.* **45**, 589–595 (2018).
28. Sakai, T. et al. Equation of state of pure iron and $Fe_{0.9}Ni_{0.1}$ alloy up to 3 Mbar. *Phys. Earth Planet. Inter.* **228**, 114–126 (2014).
29. Kamada, S. et al. The sound velocity measurements of Fe_3S. *Am. Mineral.* **99**, 98–101 (2014).
30. Kamada, S. et al. Equation of state of Fe_3S at room temperature up to 2 megabars. *Phys. Earth Planet. Inter.* **228**, 106–113 (2014).
31. McDonough, W. F. & Yoshizaki, T. Terrestrial planet compositions controlled by accretion disk magnetic field. *Prog. Earth. Planet. Sci.* **8**, 39 (2021).
32. Antonangeli, D. et al. Composition of the Earth's inner core from high-pressure sound velocity measurements in Fe-Ni-Si alloys. *Earth Planet. Sci. Lett.* **295**, 292–296 (2010).
33. Dominijanni, S. et al. Sound velocity measurements of B2-Fe-Ni-Si alloy under high pressure by inelastic x-ray scattering: Implications for the composition of Earth's core. *Geophys. Res. Lett.* **49**, e2021GL096405 (2022).
34. Fischer, R. A. et al. Equations of state in the Fe-FeSi system at high pressures and temperatures. *J. Geophys. Res.* **119**, 2810–2827 (2014).
35. Ikuta, D., Ohtani, E. & Hirao, N. Two-phase mixture of iron-nickel-silicon alloys in the Earth's inner core. *Commun. Earth Environ.* **2**, 225 (2021).
36. Allegre, C. J., Poirier, J. P., Humler, E. & Hofmann, A. W. The chemical composition of the Earth. *Earth Planet. Sci. Lett.* **134**, 515–526 (1995).
37. Chen, B., Gao, L., Funakoshi, K. & Li, J. Thermal expansion of iron-rich alloys and implications for the Earth's core. *Proc. Natl Acad. Sci. USA* **104**, 9162–9167 (2007).
38. Hirose, K., Wood, B. & Vocadlo, L. Light elements in the Earth's core. *Nat. Rev. Earth Environ.* **2**, 645–658 (2021).
39. Yokoo, S., Hirose, K., Sinmyo, R. & Tagawa, S. Melting experiments on liquidus phase relations in the Fe-S-O ternary system under core pressures. *Geophys. Res. Lett.* **46**, 5137–5145 (2019).
40. Kamada, S. et al. Phase relationships of the Fe-FeS system in conditions up to the Earth's outer core. *Earth Planet. Sci. Lett.* **359–360**, 26–33 (2012).
41. Kuwayama, Y. & Hirose, K. Phase relations in the system Fe-FeSi at 21 GPa. *Am. Mineral.* **89**, 273–276 (2004).

42. Ozawa, H., Hirose, K., Yonemitsu, K. & Ohishi, Y. High-pressure melting experiments on Fe-Si alloys and implications for silicon as a light element in the core. *Earth Planet. Sci. Lett.* **456**, 47–54 (2016).

43. Hasegawa, M., Hirose, K., Oka, K. & Ohishi, Y. Liquidus phase relations and solid-liquid partitioning in the Fe-Si-C system under core pressures. *Geophys. Res. Lett.* **48**, e2021GL092681 (2021).

44. Badro, J., Cote, A. S. & Brodholt, J. P. A seismologically consistent compositional model of Earth's core. *Proc. Natl Acad. Sci. USA* **111**, 7542–7545 (2014).

45. Prescher, C. et al. High Poisson's ratio of Earth's inner core explained by carbon alloying. *Nat. Geosci.* **8**, 220–223 (2015).

46. Takahashi, S. et al. Sound velocity of Fe_3C at high pressure and high temperature determined by inelastic x-ray scattering. *C. R. Geosci.* **351**, 190–196 (2019).

47. Shibazaki, Y. et al. Sound velocity measurements in dhcp-FeH up to 70 GPa with inelastic x-ray scattering: Implications for the composition of the Earth's core. *Earth Planet. Sci. Lett.* **313–314**, 79–85 (2012).

48. Sakamaki, K. et al. Melting phase relation of FeH_x up to 20 GPa: Implication for the temperature of the Earth's core. *Phys. Earth Planet. Inter.* **174**, 192–201 (2009).

49. Kato, C. et al. Stability of fcc phase FeH to 137 GPa. *Am. Mineral.* **105**, 917–921 (2020).

50. Tanaka, R. et al. The sound velocity of wustite at high pressures: Implications for low-velocity anomalies at the base of the lower mantle. *Prog. Earth Planet. Sci.* **7**, 23 (2020).

51. Bajgain, S. K., Mookherjee, M. & Dasgupta, R. Earth's core could be the largest terrestrial carbon reservoir. *Commun. Earth Environ.* **2**, 165 (2021).

52. Ikuta, D. et al. Interstitial hydrogen atoms in face-centered cubic iron in the Earth's core. *Sci. Rep.* **9**, 7108 (2019).

53. Wang, W. et al. Strong shear softening induced by superionic hydrogen in Earth's inner core. *Earth Planet. Sci. Lett.* **568**, 117014 (2021).

54. He, Y. et al. Superionic iron alloys and their seismic velocities in Earth's inner core. *Nature* **602**, 258–262 (2022).

55. Antonangeli, D. et al. Elastic anisotropy in textured hcp-iron to 112 GPa from sound wave propagation measurements. *Earth Planet. Sci. Lett.* **225**, 243–251 (2004).

56. Mao, W. L. et al. Experimental determination of the elasticity of iron at high pressure. *J. Geophys. Res.* **113**, B09213 (2008).

57. Ikuta, D. et al. Large density deficit of Earth's core revealed by a multi-megabar primary pressure scale. Preprint at https://arxiv.org/abs/2104.02076 (2021).

58. Seto, Y., Nishio-Hamane, D., Nagai, T. & Sata, N. Development of a software suite on x-ray diffraction experiments. *Rev. High. Press. Sci. Technol.* **20**, 269–276 (2010).

59. Seto, Y. Whole pattern fitting for two-dimensional diffraction patterns from polycrystalline materials. *Rev. High. Press. Sci. Technol.* **22**, 144–152 (2012).

60. Poirier, J. P. *Introduction to the Physics of the Earth's Interior.* 2nd edn (Cambridge University Press, 2000).

Author contributions

E.O. and A.B. devised the project. T.S. designed the stepped bevel diamond anvil and machined it with the focused ion beam (FIB) module. D. Ikuta performed the sample preparation and managed the experimental plan. D. Ikuta, E.O., H.F., D. Ishikawa, and A.B. participated in experiments. D. Ikuta analysed the data and performed the calculations. D. Ikuta, E.O., and A.B. wrote the article with input from all authors.

Competing interests

The authors declare no competing interests.

Additional information

Supplementary information The online version contains supplementary material available at https://doi.org/10.1038/s41467-022-34789-2.

Correspondence and requests for materials should be addressed to Daijo Ikuta, Eiji Ohtani or Alfred Q. R. Baron.

Peer review information *Nature Communications* thanks the anonymous reviewers for their contribution to the peer review of this work.

Reprints and permissions information is available at http://www.nature.com/reprints

Publisher's note Springer Nature remains neutral with regard to jurisdictional claims in published maps and institutional affiliations.